IEEE Access
Multidisciplinary | Rapid Review | Open Access Journal

Received August 24, 2019, accepted October 3, 2019, date of publication October 18, 2019, date of current version October 30, 2019.

Digital Object Identifier 10.1109/ACCESS.2019.2948220

Accelerating CS-MRI Reconstruction With Fine-Tuning Wasserstein Generative Adversarial Network

MINGFENG JIANG[1], ZIHAN YUAN[1], XU YANG[1], JUCHENG ZHANG[2], YINGLAN GONG[3], LING XIA[3], AND TIEQIANG LI[4,5]

[1]School of Information Science and Technology, Zhejiang Sci-Tech University, Hangzhou 310018, China
[2]Department of Clinical Engineering, The Second Affiliated Hospital, School of Medicine, Zhejiang University, Hangzhou 310019, China
[3]Department of Biomedical Engineering, Zhejiang University, Hangzhou 310027, China
[4]Institute of Informatic Engineering, China Jiliang University, Hangzhou 310018, China
[5]Division of Medical Imaging and Technology, Department of Clinical Science, Intervention and Technology, Karolinska Institutet, 171 77 Stockholm, Sweden

Corresponding author: Mingfeng Jiang (m.jiang@zstu.edu.cn)

This work was supported in part by the National Natural Science Foundation of China under Grant 61672466, Grant 61671405, and Grant 61701435, in part by the Joint Fund of Zhejiang Provincial Natural Science Foundation under Grant LSZ19F010001, in part by the Natural Science Foundation of Zhejiang Province under Grant LY17H180003, in part by the Science Technology Department of Zhejiang Province under Grant LGG18H180001, and in part by the 521 Talents project of Zhejiang Sci-Tech University.

ABSTRACT Compressed sensing magnetic resonance imaging (CS-MRI) is a time-efficient method to acquire MR images by taking advantage of the highly under-sampled k-space data to accelerate the time consuming acquisition process. In this paper, we proposed a de-aliasing fine-tuning Wasserstein generative adversarial network (DA-FWGAN) for imaging reconstruction of highly under-sampled k-space data in CS-MRI. In the architecture, we used the fine-tuning method for accurate training of the neural network parameters and the Wasserstein distance as the discrepancy measure between the real and reconstructed images. Furthermore, for better preservation of the fine structures in the reconstructed images, we incorporated perceptual loss, image and frequency loss into the loss function for training the network. With experimental results from 3 different sampling schemes and 3 levels of sampling rates, we compared the reconstruction performance of the DA-FWGAN method with other state-of-the-art deep learning methods for CS-MRI reconstruction, including ADMM-Net, Pixel-GAN, and DAGAN. The proposed DA-FWGAN method outperforms all other methods and can provide superior reconstruction with improved peak signal-to-noise ratio (PSNR) and structural similarity index measure.

INDEX TERMS Fine-tuning, image reconstruction, magnetic resonance image (MRI), Wasserstein generative adversarial network (WGAN).

I. INTRODUCTION

Magnetic Resonance Imaging (MRI) is a widely used medical image technology [1]–[3] and can provide non-invasive diagnostic imaging of the tissue structures in the human body. With MRI, we acquire the k-space data [4] in the time domain and perform the image reconstruction using inverse fast Fourier transformation (FFT) to generate real-space images in the frequency domain. MRI does not involve exposure to ionizing radiation, and thus avoids the associated carcinogenic risk. However, the scanning time to acquire high-resolution images can be too long for some patients to endure the discomfort of keeping the same posture. In addition, imaging quality is susceptible to physiological movements and motion artifacts. Therefore, how to accelerate the acquisition speed and improve the quality of MRI has been one of the important research topics in MRI. The current promising technologies for fast MRI include mainly CS-MRI based methods [5], such as graph-based redundant wavelet transform [6], pseudo-polar [7], CS-MRI reconstruction using GPUs [8], multi-contrast guided graph representation [9], CS-MRI reconstruction via group-based eigenvalue decomposition and estimation [10], and CS-MRI with phase noise disturbance based on adaptive tight frame and total variation [11].

The associate editor coordinating the review of this manuscript and approving it for publication was Wei Chen.

Other development directions include the combination methods of parallel imaging with compressed sensing, such as k-t Sparse SENSE [12], iGRASP [13], learning joint-sparse codes for calibration-free parallel MR imaging [14], low-rank model for MRI, using redundant wavelet tight frame [15], and dictionary learning based reconstruction methods [16]–[19].

Recently, the deep learning method [20] has received great attention. Because of its breakthroughs in computer vision, it has found applications in areas such as super-resolution imaging [21], denoising, image inpainting [22], and reconstruction [23]. Particularly, transfer learning [24] has become a promising method to transfer the parameters of a trained model to a new model, so as to speed up the learning efficiency of the optimized model. Fine-tuning [25] is one of the commonly used transfer learning methods, which starts directly with a pre-trained deep neural network to seek ''worthy'' samples, which are then continuously fine-tuned further by incorporating newly annotated samples in each iteration to enhance the network performance incrementally.

At present, the deep learning based methods have been applied to image reconstruction in MRI [26], [27], including two mainly different network structures: the convolutional neural networks (CNN) and generative adversarial network (GAN). Wang *et al.* [28] designed and trained an offline CNN to map the relationship between the MR images reconstructed from the under- and fully-sampled k-space data. For the first time, CNN was successfully applied to MRI reconstruction. Once the CNN model is trained, highly undersampled k-space data can be reconstructed quickly and accurately by using the CNN model. The reconstructed image is quite similar to the corresponding fully sampled image. In addition, a deep cascade of convolutional neural networks (CNNs) was proposed for reconstructing dynamic sequences of 2D cardiac MR images from undersampled data [29], which can accelerate the data acquisition process significantly. Deep learning networks have also been used to initialize the classic CS-MRI either in a two-stage reconstruction or integrating directly into the CS-MRI reconstruction as an additional regularization term [30]. To improve the reconstruction accuracy and computational speed for CS-MRI, Yang *et al.* [31] developed a novel deep architecture, ADMM-Net, which was defined over a data flow graph and derived from the iterative procedures in Alternating Direction Method of Multipliers (ADMM) algorithm [32]. It has been reported that the ADMM-Net method can significantly improve the baseline ADMM algorithm and achieve high accuracy reconstruction with fast computational speed. In summary, compared with traditional CS-MRI methods, the CNN-based reconstruction methods have potential to reduce the MRI scanning time, speed up the reconstruction and improve the imaging quality.

With the development of deep learning technology, the Generative Adversarial Network (GAN) proposed by Goodfellow *et al.* [33], has recently been demonstrated to have good performance in image transformation [34] and super-resolution imaging [35]. More recently, deep de-aliasing generative adversarial network method (DAGAN) has been implemented for fast CS-MRI [36]. Accumulating evidence shows that GAN-based methods can achieve better image quality than ADMM-Net methods. As one of the variant network structures, Wasserstein GAN [37] has been developed to tackle the problem of network training instability, which is believed to be associated with the existence of undesirable sharp gradients of the GAN discriminator function. Yang *et al.* [38] adopted Wasserstein GAN for denoising low-dose CT images and attained a successful application in medical imaging reconstruction. The recent study by Antun *et al.* [39] also underscores the importance of stability in using deep learning network for CS-MRI reconstruction. Deep learning method can work well in an enclosed condition, therefore, undetectable perturbations will cause unpredictable reconstruction results. Some constraints are an effective way to solve this issue. Overall, the deep learning method is a promising way for accelerating MR image reconstruction.

In this study, we proposed a novel de-aliasing fine-tuning Wasserstein generative adversarial network (DA-FWGAN) for CS-MRI reconstruction, which can further improve the reconstruction performance of DAGAN method. The generator was designed as three U-Net [40], [41] neural network architecture with refinement learning and skip connections [42]. The purpose of the three U-Net is to train the generator model from coarse to fine. In addition, the discriminator built in the CNN architecture does not include the sigmoid layer. The discriminator loss function was converted to the Wasserstein distance [43], [44] between the real and reconstructed images. Perceptual loss, the image and frequency loss were also incorporated into the loss function [35] in order to enhance the quality of the reconstructed image. Moreover, root mean square propagation (RMSProp) was proposed to optimize the loss function.

II. METHODS

A. LINKED NEURAL NETWORK TO CS-MRI

If we denote $\mathbf{X} \in \mathbb{C}^{N\times N}$ as the reconstruction image and $\mathbf{Y} \in \mathbb{C}^{N\times N}$ as the undersampled k-space data [45], the CS-MRI reconstruction can be formulated as follows:

$$\mathbf{Y} = \mathbf{F_u}\mathbf{X} + \varepsilon \tag{1}$$

where $\mathbf{F_u}$ presents Fourier transformation operation matrix with under-sampled mask, ε means the noise. In the traditional CS-MRI algorithm, a-priori information is always used to overcome the ill-posed property of the image reconstruction so as to reconstruct accurately the image $\mathbf{X}$ from undersampled k-space data $\mathbf{Y}$. Recently, neural networks have been incorporated as constraints to obtain a unique solution for the reconstruction problem [28], [36], which can be formulated in the following way:

$$\min_{\mathbf{x}} \frac{1}{2}\left\|\mathbf{F_u}\mathbf{X} - \mathbf{Y}\right\|_2^2 + \varphi R(\mathbf{X}) + \lambda \left\|\mathbf{X} - f_{nn}\left(\mathbf{Z}|\theta^*\right)\right\|_2^2 \tag{2}$$

where $\frac{1}{2}\left\|\mathbf{F_u}\mathbf{X} - \mathbf{Y}\right\|_2^2$ is the data fidelity term, $R(\mathbf{X})$ represents regularization term, and φ is a regularization parameter

in CS-MRI. $\mathbf{Z}$ is the zero-filled reconstruction from the under-sampled k-space measurements $\mathbf{Y}$. $f_{nn}(\mathbf{Z}|\theta^*)$ represents the image generated by the neural networks, θ^* represents the optimal parameters of the trained neural networks, and λ is the regularization parameter.

B. FROM GAN TO WGAN

The original GAN networks are deep neural network architectures comprised of two nets: a generator G and a discriminator D. In the context of CS-MRI reconstruction, the generator continuously learns the true probability distribution of the training data, $\mathbf{X}$, and zero-filled undersampled reconstructed images, $\mathbf{Z}$, to mimic the true probability distribution. That is, the generated full MR image from a zero-filling reconstruction (i.e., image generated from under-sampled k-space data) is within a small distance to the fully sampled image and the generator targets to make the discriminator unable to discern if the image is real or generated. The discriminator distinguishes whether the reconstructed image by the generator conforms to the fully sampled real image, thereby, identifies if the output result is real or reconstructed. Mathematically, it can be formulated as a minimax game, and the ultimate goal is to achieve a Nash equilibrium. The MRI reconstruction problem is to generate images, which are equal to the fully sampled real image. This can be expressed as follows [36]:

$$\min_G \max_D L(D, G) = E_{\mathbf{X}\sim P_{\text{data}}(\mathbf{X})}[\log D(\mathbf{X})] + E_{\mathbf{Z}\sim P_Z(\mathbf{Z})}[\log(1 - D(G(\mathbf{Z})))] \quad (3)$$

where E represents mathematical expectation, and $P_{\text{data}}(\mathbf{X})$ is the real data distribution.

Let $P_G(\mathbf{X})$ be the distribution induced by the generator, for a fixed generator, the optimal discriminator is

$$D^*(\mathbf{X}) = \frac{P_{data}(\mathbf{X})}{P_{data}(\mathbf{X}) + P_G(\mathbf{X})} \text{ st. } P_{data}(\mathbf{X}) = P_G(\mathbf{X}) \quad (4)$$

when the discriminator is optimal, the minimax game is reduced into a minimization over the generator as follows [33]:

$$\min_G L\left(D^*, G\right) = \text{JSD}\left(P_{\text{data}} \| P_G\right) - \log(2) \quad (5)$$

As shown in (5), the more the discriminator becomes trained, the more the generator gradient disappears. The Jensen-Shannon divergence (JSD) [47] is abrupt in the original GAN and is either maximal or minimum, whereas the Wasserstein distance is smooth and can avoid the gradient disappearance problem to improve the training stability. JSD can lead to instability in network training and mode collapse. Wasserstein GAN provides an effective way to overcome this issue. In this study, the Wasserstein distance (aka Earth-Mover distance) is used to reflect the gap between P_G and P_{data} [46] according to following formula

$$W(P_{data}, P_G) = \inf_{\gamma\sim\Pi(P_{\text{data}}, P_G)} E_{(\mathbf{X},\mathbf{Z})\sim\gamma}[\|\mathbf{X} - \mathbf{Z}\|] \quad (6)$$

The function of the network is to learn continuously from the mapping $G : \mathbf{Z} \rightarrow \mathbf{X}$, which generates MR images from undersampled and zero-filled MR data. The gap between the real and reconstructed image becomes smaller and smaller over the training process. The optimal reconstruction model can be approached by continuously adjusting the parameters in the neural network through a large number of samples. The JSD was used as evaluation criterion in the loss function of the original GAN. To mitigate the gradient disappearance in the WGAN based reconstruction model, the evaluation criterion is formulated as the following:

$$\min_G \max_D L_{WGAN}(D, G) = -E_{\mathbf{X}\sim P_{\text{data}}(\mathbf{X})}[D(\mathbf{X})] + E_{\mathbf{Z}\sim P_Z(\mathbf{Z})}[D(G(\mathbf{Z}))] \quad (7)$$

C. CONTINUOUS FINE-TUNING

Transfer learning is an effective way to solve the problem with a small training sample and use the pre-trained model to improve the generalization ability of the network. In this work, we combined transfer learning with fine-tuning method. The procedure of fine-tuning is continuous training from coarse to fine. The coarse procedure is to pre-train the model (the first two layers of U-Net of the generator) with a small sample size. And the fine procedure is to continuously fine-tune the whole model with the augmented datasets on top of the pre-trained model in an incremental fashion until the performance is satisfactory. The difference between the fine-tuning method and training from scratch is that the former uses the trained parameters to initialize and the latter achieves initialization according to the way specified by the network. With the proposed DA-FWGAN architecture, the fine-tuning method can shorten the convergence time and significantly improve the quality of the generated images, especially when the target dataset is small.

D. LOSS FUNCTION

The loss function provides a measure to estimate the gap between the real and reconstructed MR image. The smaller the loss function value is, the more robust the DA-FWGAN model becomes. In order to improve the quality of the reconstruction, we proposed to incorporate the perceptual loss, image domain mean square error (iMSE), frequency domain mean squared error (fMSE), and the adversarial loss together as the loss function of the generator [36].

First, the iMSE and fMSE based loss functions can be formulated as

$$\min_G L_{iMSE}(G) = \frac{1}{2}\|\mathbf{X}_{\text{t}} - \mathbf{X}_{\text{u}}\|_2^2 \quad (8)$$

$$\min_G L_{fMSE}(G) = \frac{1}{2}\left\|\widehat{\mathbf{Y}}_{\text{t}} - \widehat{\mathbf{Y}}_{\text{u}}\right\|_2^2 \quad (9)$$

where $\mathbf{X}_{\text{t}}$ and $\mathbf{X}_{\text{u}}$ are fully sampled and reconstructed MR images, respectively. $\widehat{\mathbf{Y}}_{\mathbf{t}}$ and $\widehat{\mathbf{Y}}_{\mathbf{u}}$ correspond to the frequency domain data of $\mathbf{X}_{\text{t}}$ and $\mathbf{X}_{\text{u}}$, respectively. The perceptual loss and adversarial loss are defined as

$$\min_G L_{VGG}(G) = \frac{1}{2}\|f_{VGG}(\mathbf{X}_{\text{t}}) - f_{VGG}(\mathbf{X}_{\text{u}})\|_2^2 \quad (10)$$

$$\min_G L_{GEN}(G) = E_{\mathbf{Z}\sim P_Z(\mathbf{Z})}[D(G(\mathbf{Z}))] \tag{11}$$

where f_{VGG} is VGG16 network [48]. $P_Z(\mathbf{Z})$ is the distribution of the reconstructed MR images. So, the combined loss function can be presented as

$$L_{conbine} = \alpha L_{iMSE} + \beta L_{fMSE} + \delta L_{VGG} + L_{GEN} \tag{12}$$

E. PROPOSED NETWORK

The key idea for the proposed DA-FWGAN approach is to introduce Wasserstein distance as the new evaluation criterion in GAN-based MRI reconstruction and use fine-tuning method for the training of the model from coarse to fine. Similar to the original GAN network, the overall network architecture is divided into two parts: generator and discriminator. The generator is designed as three cascading U-Net CNN architectures with refinement learning and skips connections. The first U-Net consists of 4 convolution layers (encoder) and 4 deconvolution layers (decoder); the second consists of 6 convolution layers and 6 deconvolution layers, and the last U-Net set includes 8 convolution layers and 8 deconvolution layers. The discriminator is a CNN architecture without the sigmoid layer. To assess the similarity degree between the real and reconstructed images we calculate the Wasserstein distance between them. The updated values of discriminator parameters are truncated to a small range to overcome the issue of gradient disappearance. The perceptual loss, image loss, and frequency loss are also incorporated into the loss function to enhance the output quality from the generator. Moreover, the generator target is converted to minimize the Wasserstein distance and RMSProp is used to optimize the loss function. Specifically, the generator and discriminator are trained alternatively by fixing one and updating the other. The proposed network architecture is schematically shown in Fig. 1.

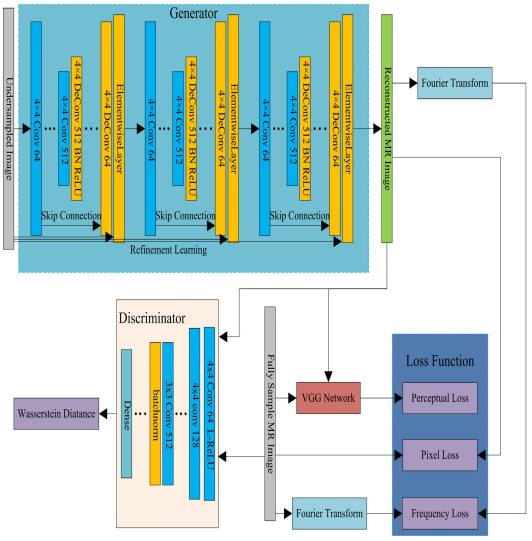

FIGURE 1. Schematics of the proposed DA-FWGAN architecture.

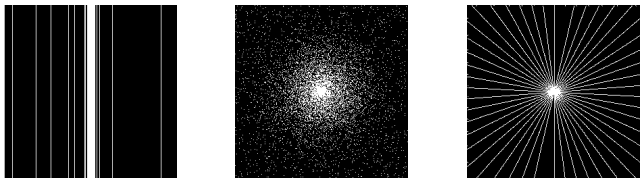

FIGURE 2. The three different under sampling masks, from left to right are: the 1D Gaussian mask(a), 2D Gaussian mask(b), and radial sampling mask(c).

III. EXPERIMENTS

A. EXPERIMENTAL PROCEDURES AND ANALYSIS METHODS

The diencephalon challenge dataset of the MICCAI 2013 grand challenge (https://www.synapse.org/#!Synapse:syn3193805/wiki/217780) [36] was used to train and test the DA-FWGAN model. During the training procedure, a small number of training samples were introduced to train the first two U-Nets of the network, and then datasets of two different sizes were used to train the rest of the network. Therefore, three datasets of different sizes were used to train the network model. The first batch consisted of 30 randomly selected 3D MRI datasets and was used as the pre-training sets. 70% (5000 effective 2D images) were used as training samples and 30% (2100 effective 2D image) as validation samples. The second batch consisted of 100 randomly selected 3D MRI datasets and was used as training sets. The training and validation samples were 70% (15800 effective 2D images) and 30% (6700 effective 2D images), respectively. The third batch was the same size as the first one. In this report, two different independent tests were conducted to validate the performances of the proposed DA-FWGAN model.

Three different under sampling masks were proposed to acquire the k-space data, i.e., 1D Gaussian distribution, 2D Gaussian distribution and radial mask, as shown in Fig. 2. Different sampling rates of 10%, 20%, and 30% were introduced to evaluate the reconstruction performance of the different methods. The selected sampling rates represent 10, 5, and 3.3 folds of acquisition accelerations, respectively.

Both the peak signal-to-noise ratio (PSNR) and structural similarity index measure (SSIM) were used to evaluate the quality of reconstructed MR image.

$$PSNR = 10\log_{10}\left(\frac{255^2}{MN\sum_{i=1}^{M}\sum_{j=1}^{N}(y_{i,j}-x_{i,j})^2}\right) \tag{13}$$

where x is the fully sampled image, y is the reconstructed image for the under samplings, i and j are the coordinates of the pixels and the size of the image is $M \times N$

$$SSIM = \frac{(2\mu_x\mu_y + C_1)(2\sigma_{xy} + C_2)}{(\mu_x^2 + \mu_y^2 + C_1)(\sigma_x^2 + \sigma_y^2 + C_2)} \tag{14}$$

where μ_x and μ_y are the means for the images x, y respectively. σ_x and σ_y are the image variances of x, y, respectively.

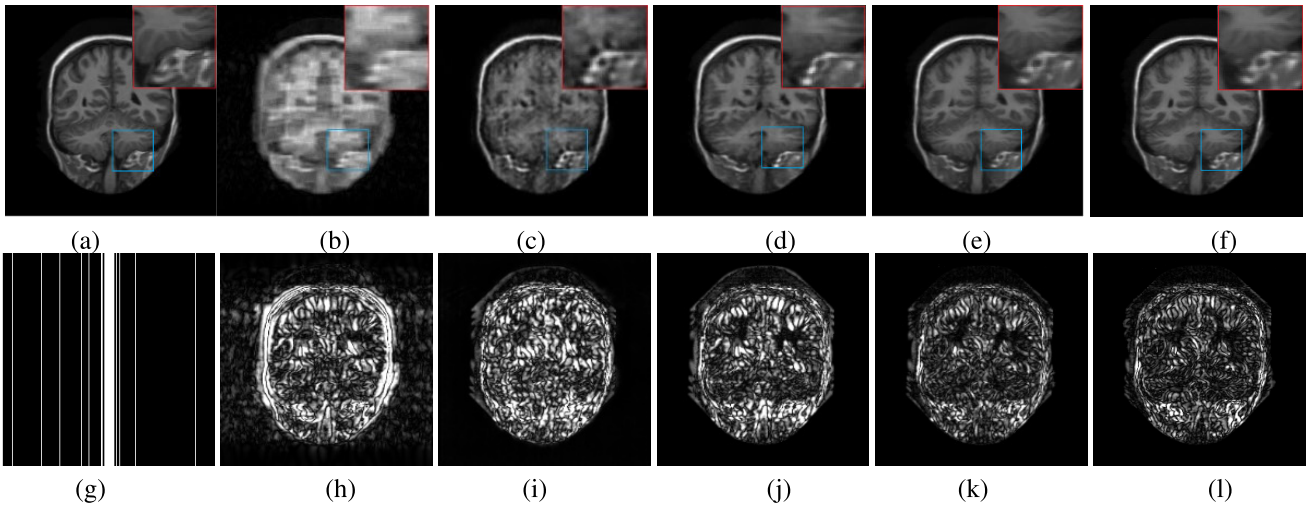

FIGURE 3. The reconstruction results for the 10-fold accelerated k-space data masked with the 1D Gaussian distribution. In the first row, from left to right are the fully sampled grand-truth MR image (a), and the under-sampled reconstruction results obtained using ADMM-Net (b), Pixel-GAN (c), DAGAN (d), DA-WGAN (e), and DA-FWGAN (f). In the 2nd row, from left to right are the 1D Gaussian mask (g), and the corresponding residual images for ADMM-Net (h), Pixel-GAN (i), DAGAN (j), DA-WGAN (k), and DA-FWGAN (l). The framed square region indicates the zoom insert.

σ_{xy} is the covariance of x and y. The constant values C_1 and C_2 are used to maintain stability and are determined by simplified calculation formula.

$$C_1 = (k_1 L)^2 \tag{15}$$

$$C_2 = (k_2 L)^2 \tag{16}$$

where k_1 is 0.01 and k_2 is 0.03. L is the dynamic range of pixel values.

To avoid contingency caused by single analysis approach. Two independents analysis methods were used to assess the reconstruction performance of the proposed deep learning method. One is to compute the average quality metrics: PSNRs and SSIMs, for all the reconstructed images (5200 effective 2D image samples) and the other is to select and evaluate a representative image out of the testing examples.

B. NETWORK TRAINING SETTINGS

A server, based on Intel(R) Xeon(R) Gold 6148 CPU and Tesla V100-SXM2 GPU was configured using the CentOS system. Python and TensorFlow frameworks were the development environments.

The DA-FWGAN network was trained to reconstruct images from k-space data with different levels of undersampling rates. We used the following fixed mutual hyperparameters: the batch size of 16, the initial learning rate of 0.0001, and the learning rate attenuation factor of 0.5. The α, β, and δ parameters in the loss function were set to 15, 0.1, and 0.0025, respectively. The learning rate was updated every 5 epochs. The update range of discriminator parameter was 0.01.

We took advantage of the VGG16 network architecture and used a pre-trained model and its function for perceptual loss [48]. In order to avoid over-fitting, the normalized mean square error (NMSE) was utilized as the criterion to determine the optimal model. If the current NMSE is smaller than those found in the next 10 epochs, then we would stop training the network further and save the current model as the optimal model.

IV. RESULTS

As stateded above, a batch of 3D MRI samples of three different sampling masks were used to train the GAN model. After training the model, samples of different sizes were tested to validate the reconstruction performances of the proposed DA-FWGAN method. The qualitative performance of the DA-FWGAN method (in terms of visual inspection for the reconstructed MR images) and quantitative metrics of the reconstruction results (in terms of PSNR and SSIM) were compared to other state-of-the-art deep learning methods.

As shown in Fig. 3, in comparison with the fully sampled grand-truth image (Fig. 3a) the reconstructed images for the k-space data with 10% sampling rate depict various degrees of artifacts, which is apparent by visual inspection of the images and their corresponding residual images. It is evident that the reconstruction quality for the ADMM-Net (Fig. 3b) and Pixel-GAN (Fig. 3c) are quite poor and the structural details are lost seriously. Although the reconstruction quality for the DAGAN method (Fig. 3d) is somewhat improved, there is still significant loss of structural information and the edges of the image are too smooth. In contrast, the reconstruction qualities for the DA-WGAN (Fig. 3e) and DA-FWGAN (Fig. 3f) methods are substantially improved, as indicated by the reduced residual amplitudes (see Figs. 3k and 3l). The proposed DA-FWGAN method preserves more detailed structural information. The reconstructed image (Fig. 3f) has clear texture details and most of the aliasing artifacts are effectively suppressed even with 10-fold acquisition acceleration.

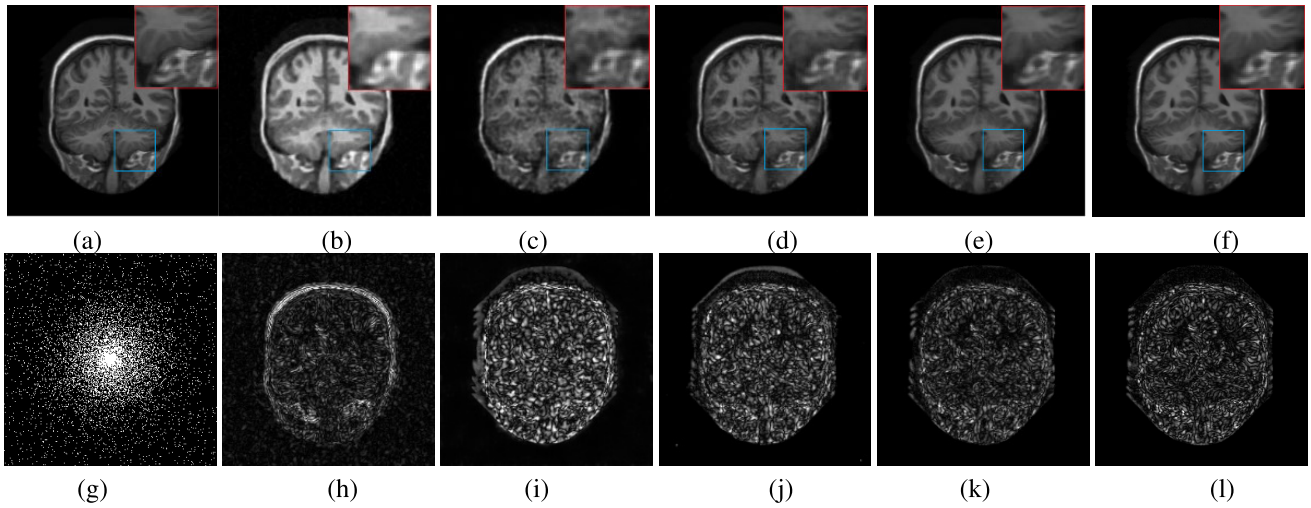

FIGURE 4. The reconstruction results for the 10-fold accelerated k-space data masked with the 2D Gaussian distribution. In the first row, from left to right are the fully sampled grand-truth MR image (a), and the under-sampled reconstruction results obtained using ADMM-Net (b), Pixel-GAN (c), DAGAN (d), DA-WGAN (e), and DA-FWGAN (f). In the 2nd row, from left to right are the 2D Gaussian mask (g), and the corresponding residual images for ADMM-Net (h), Pixel-GAN (i), DAGAN (j), DA-WGAN (k), and DA-FWGAN (l).

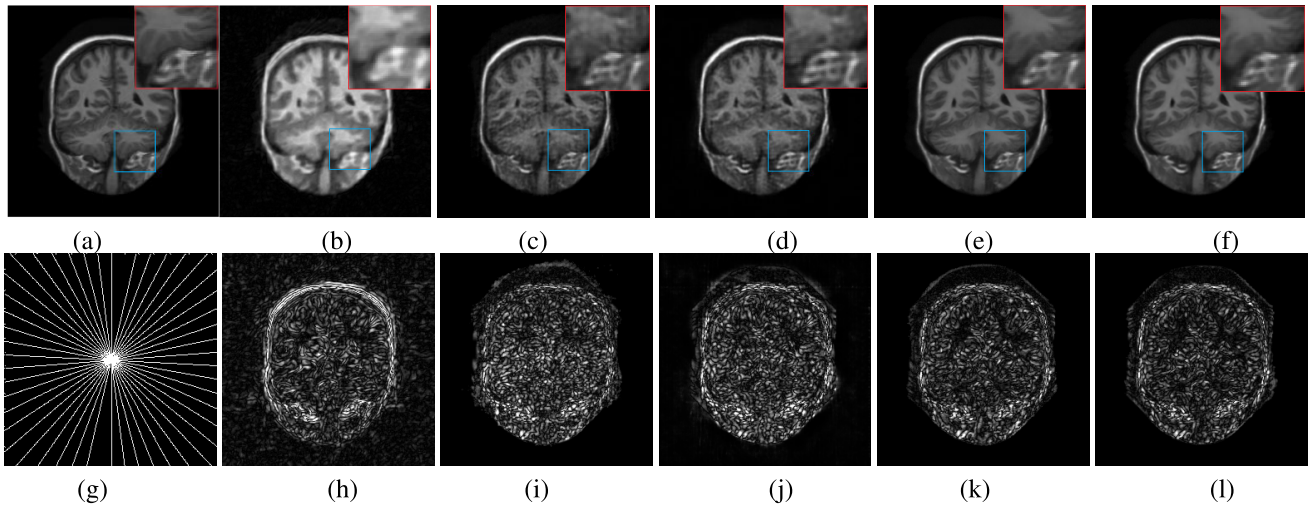

FIGURE 5. The reconstruction results for the 10-fold accelerated k-space data masked with the 2D radial sampling. In the first row, from left to right are the fully sampled grand-truth MR image (a), and the under-sampled reconstruction results obtained using ADMM-Net (b), Pixel-GAN (c), DAGAN (d), DA-WGAN (e), and DA-FWGAN (f). In the 2nd row, from left to right are the 2D radial mask (g), and the corresponding residual images for ADMM-Net (h), Pixel-GAN (i), DAGAN (j), DA-WGAN (k), and DA-FWGAN (l).

As shown in Fig. 4, we have obtained similar results for the 10-fold accelerated k-space sampling masked with a 2D Gaussian distribution. The WGAN based methods perform better than the other three methods, and DA-FWGAN outperforms DA-WGAN method slightly. Furthermore, compared to the 1D Gaussian mask with the same sampling coverage, the sampling scheme based on a 2D Gaussian mask provides significantly better image quality, as expected from the fact that the 2D Gaussian mask acquires more data points in the center of k-space.

The reconstructed MR images by using different methods with 10% radial sampling mask are presented in Fig. 5. It can be found that, with highly under-sampled radial mask, the proposed DA-FWGAN method outperforms all other reconstruction methods and can reconstruct the MR image with clearer border. Moreover, compared with other two under-sampling masks, the reconstruction results of radial sampling are superior to the 1D Gaussian reconstruction results, and comparable to the 2D Gaussian reconstruction results.

In addition to the qualitative comparison of the reconstruction performances discussed above, the quantitative analyses of the quality metrics also confirm the superior performance of the proposed DA-FWGAN method. Table 1 shows the average SSIM and PSNR results for all the testing samples of 5200 images. The SSIM and PSNR values for a

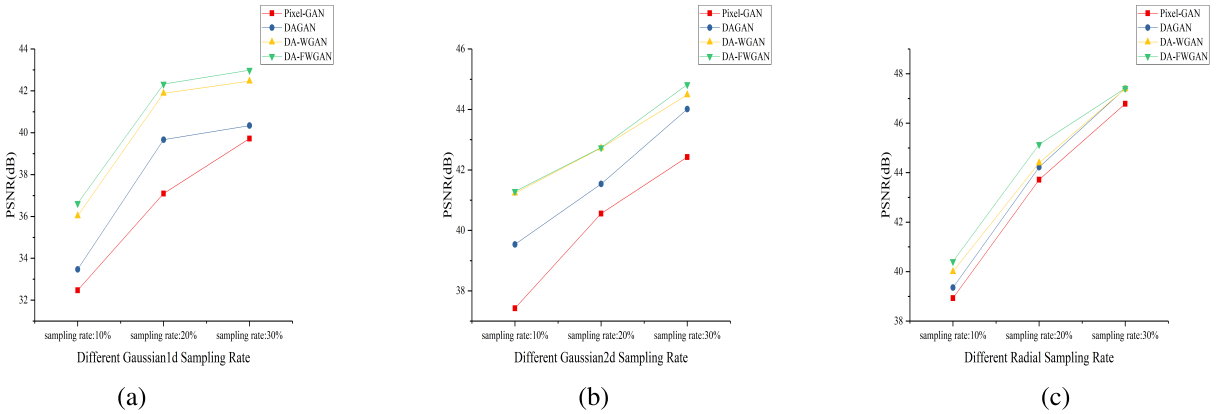

FIGURE 6. Average PSNR as a function of the under-sampling rate of k-space data for 1D Gaussian(a), 2D Gaussian(b) and radial(c) sampling masks.

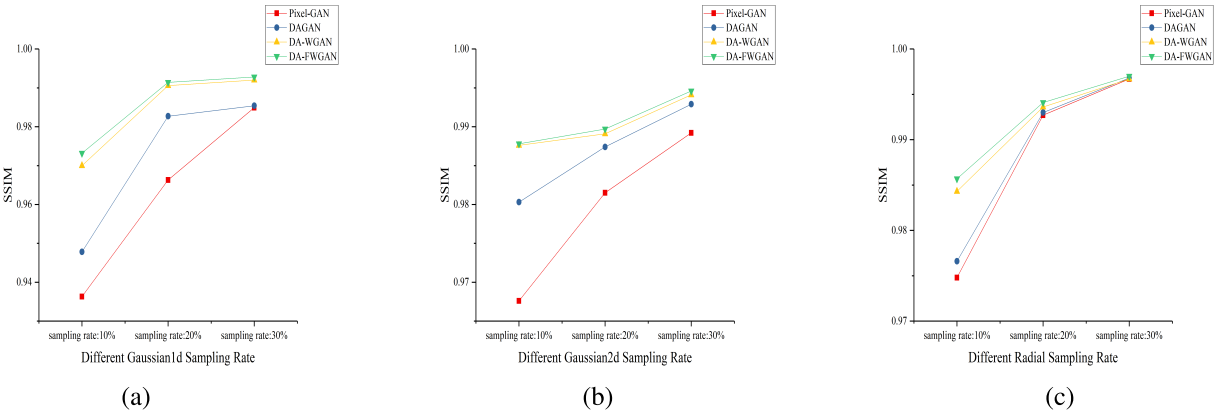

FIGURE 7. Average SIMM as a function of the under-sampling rate of k-space data for 1D Gaussian(a), 2D Gaussian(b) and radial(c) sampling masks.

TABLE 1. The average reconstruction performances of 25 randomly selected 3D MRI (5200 effective 2D) images.

15800 images	ADMM-Net		Pixel-GAN		DAGAN		DA-WGAN		DA-FWGAN	
mask: 1D Gaussian	SSIM	PSNR	SSIM	PSNR	SSIM	PSNR	SSIM	PSNR	SSIM	PSNR
sample rate: 10%	0.5874	24.4447	0.9363	32.4700	0.9478	33.4711	0.9700	36.0302	**0.9732**	**36.6258**
sample rate: 20%	0.8407	33.4952	0.9663	37.0970	0.9827	39.6682	0.9906	41.8865	**0.9914**	**42.3225**
sample rate: 30%	0.8759	33.9099	0.9849	39.7230	0.9854	40.3395	0.9920	42.4669	**0.9928**	**42.9831**
mask:2D Gaussian	SSIM	PSNR	SSIM	PSNR	SSIM	PSNR	SSIM	PSNR	SSIM	PSNR
sample rate: 10%	0.6883	32.9278	0.9676	37.4224	0.9803	39.5367	0.9876	41.2353	**0.9878**	**41.2882**
sample rate: 20%	0.8770	35.5798	0.9815	40.5581	0.9874	41.5351	0.9891	42.7260	**0.9897**	**42.7345**
sample rate: 30%	0.8816	38.6711	0.9892	42.4237	0.9929	44.0110	0.9941	44.4851	**0.9946**	**44.8233**
mask:Radial	SSIM	PSNR	SSIM	PSNR	SSIM	PSNR	SSIM	PSNR	SSIM	PSNR
sample rate: 10%	0.5772	30.0294	0.9748	38.9304	0.9766	39.3554	0.9843	40.0002	**0.9857**	**40.4086**
sample rate: 20%	0.6435	32.2843	0.9927	43.7142	0.9930	44.2218	0.9936	44.3933	**0.9941**	**45.1404**
sample rate: 30%	0.8207	37.2010	0.9967	46.7836	0.9968	47.4003	0.9967	47.3890	**0.9970**	**47.4116**

representative image are also shown in Table 2. For comparison, we listed systematically all results for the SSIM and PSNR metrics for the 5 different reconstruction methods, three sampling masks (1D Gaussian, 2D Gaussian, and radial) and 3 levels of sampling rates (10, 20, and 30% k-space coverage). Among these five different deep learning methods, both the average and represent results demonstrate that DA-FWGAN method provides the highest reconstruction quality in all cases irrespective of the k-space sampling schemes and coverage. For more indicative view of the reconstruction quality, the average results for PSNR and SSIM are also presented as the scattered plots in Figs. 6 and 7, respectively. As shown, under the same sampling mask, the reconstruction performance becomes better with higher PSNR and SSIM, when increasing the sampling rate. The ability of DA-FWGAN to reconstruct under-sampled MR

TABLE 2. The reconstruction performance of a representative MR image.

15800 images	ADMM-Net		Pixel-GAN		DAGAN		DA-WGAN		DA-FWGAN	
mask: 1D Gaussian	SSIM	PSNR	SSIM	PSNR	SSIM	PSNR	SSIM	PSNR	SSIM	PSNR
sample rate: 10%	0.5083	21.8543	0.9067	29.4675	0.9192	30.4443	0.9529	33.1742	**0.9578**	**33.5980**
sample rate: 20%	0.7737	29.7793	0.9511	33.8538	0.9766	36.6496	0.9873	39.3854	**0.9883**	**39.8302**
sample rate: 30%	0.8385	30.4982	0.9700	37.2515	0.9785	37.4340	0.9882	39.9706	**0.9895**	**40.5477**
mask:2D Gaussian	SSIM	PSNR	SSIM	PSNR	SSIM	PSNR	SSIM	PSNR	SSIM	PSNR
sample rate: 10%	0.6882	29.7207	0.9432	33.0286	0.9599	34.8966	0.9757	37.0342	**0.9774**	**37.3044**
sample rate: 20%	0.8358	31.3558	0.9685	36.3973	0.9748	36.8978	0.9759	38.2438	**0.9805**	**38.6144**
sample rate: 30%	0.8260	34.1284	0.9792	37.5271	0.9855	39.3193	0.9879	40.2618	**0.9893**	**40.7805**
mask:Radial	SSIM	PSNR	SSIM	PSNR	SSIM	PSNR	SSIM	PSNR	SSIM	PSNR
sample rate: 10%	0.5945	27.1908	0.9522	34.0391	0.9556	34.2499	0.9710	35.6168	**0.9732**	**36.0560**
sample rate: 20%	0.7319	30.7167	0.9852	39.3266	0.9866	39.3289	0.9871	40.0499	**0.9893**	**40.5441**
sample rate: 30%	0.8102	34.0683	0.9932	42.6113	0.9939	43.4012	0.9934	42.8081	**0.9942**	**43.6631**

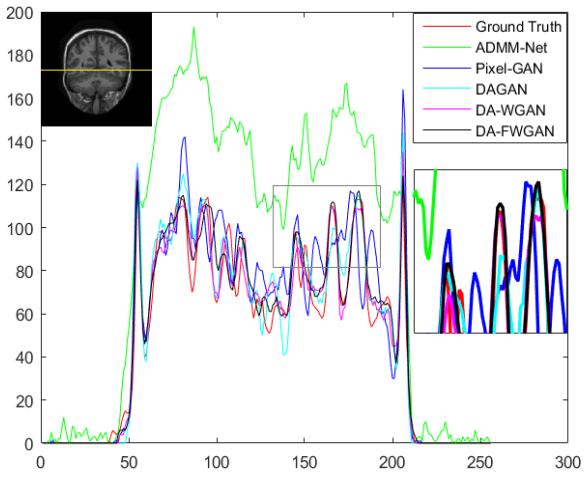

FIGURE 8. Comparison of horizontal line profiles of the reconstructed images using different deep learning methods. The k-space data were sampled with 10-fold acceleration according to the 1D Gaussian distribution.

data is consistently higher than the other methods, especially at 10% low sampling rate.

Besides the global metrics discussed above, the local features of the reconstructed image confirm further the ability for WGAN-based methods to reconstruct under-sampled MRI data. Fig. 8 displays horizontal line profiles for the reconstructed images at an arbitrarily selected location inside the brain. As shown, the image reconstructed by ADMM-Net deviates far from the ground truth result. The result of Pixel-GAN is better than ADMM-Net, but its intensity profile is substantially different from the ground truth. Compared with DAGAN method, WGAN based methods (DA-WGAN and DA-FWGAN) suppress more effectively the aliasing artifacts and produce line profiles that are more consistent with the ground-truth result.

V. DISCUSSION

The most important motivation for this study is to reconstruct highly under-sampled MRI k-space data accurately, which can shorten the scanning time effectively. With the experimental results discussed above, we have demonstrated that the proposed DA-FWGAN method can improve the reconstructed image quality and reduce the aliasing artifacts even for cases of highly under-sampled k-space data. In the DA-FWGAN architecture, we proposed to use fine-tuning method for training the neural network and the Wasserstein distance as the discrepancy measure between the real and reconstructed images. Furthermore, to better preserve the fine anatomic structures, such as texture and edges in the reconstructed images, we incorporated the perceptual loss, image and frequency domain errors into the loss function to assess the network training. Compared with the other state-of-the-art deep learning methods for CS-MRI reconstruction, such as ADMM-Net, Pixel-GAN, and DAGAN, the DA-FWGAN method can provide outstanding performance in under-sampled MRI reconstruction and generate MRI images with superior PSNR, less aliasing artifacts, and higher SSIM.

Transfer learning method is an effective way to solve the small training sample problem in deep learning methods, and fine-tuning is one of the commonly used transfer-learning methods. In this study, we investigated the effect of training sample sizes on the reconstruction of under-sampled MRI data. We explored preliminarily two different training sample sizes: 5000 versus 15800 effective 2D images, to investigate the training affect on the WGAN network model and the reconstruction of under-sampled k-space MRI data. In Table 3, we have summarized how the average PSNR and SSIM metrics of the reconstructed images are affected. As shown, increasing the training sample size by a factor of over 3 can improve the average PSNR of the reconstructed images by about 1.2-1.8% and SSIM by about 0.1-0.5%, depending on the k-space sample rates. Even though this is a relatively minor effect, it indicates that increasing training samples for the WGAN network model improves generalizability and can rerconstruct more accurately to generate images with higher PSNR and SSIM.

We have also conducted the convergence analyses in every epoch by using DAGAN, DA-WGAN, and DA-FWGAN methods in the case of 10% sampling rate with 1D Gaussian mask. As shown in Fig. 9, the convergence of DAGAN method is quite unstable and does not achieve its optimal reconstruction conditions before the 5 th epoch and the results are far from optimal when compared with the other methods. On the other hand, the convergences of DA-WGAN and

TABLE 3. Average results for randomly select 25 datasets of 3D MR images (5200 effective 2d images).

	DA-FWGAN (15800)		DA-WGAN (15800)		DA-FWGAN (5000)		DA-WGAN (5000)	
mask: 1D Gaussian	SSIM	PSNR	SSIM	PSNR	SSIM	PSNR	SSIM	PSNR
sample rate: 10%	**0.9732**	**36.6258**	0.9700	36.0302	**0.9684**	**35.8751**	0.9650	35.2855
sample rate: 20%	**0.9914**	**42.3225**	0.9906	41.8865	**0.9899**	**41.7748**	0.9898	41.3945
sample rate: 30%	**0.9928**	**42.9831**	0.9920	42.4669	**0.9913**	**42.1238**	0.9901	41.6034
mask:2D Gaussian	SSIM	PSNR	SSIM	PSNR	SSIM	PSNR	SSIM	PSNR
sample rate: 10%	**0.9878**	**41.2882**	0.9876	41.2353	**0.9853**	**40.4790**	0.9825	39.5549
sample rate: 20%	**0.9897**	**42.7345**	0.9891	42.7260	**0.9878**	**42.0894**	0.9869	41.0092
sample rate: 30%	**0.9946**	**44.8233**	0.9941	44.4851	**0.9938**	**44.3027**	0.9924	43.2454
mask:Radial	SSIM	PSNR	SSIM	PSNR	SSIM	PSNR	SSIM	PSNR
sample rate: 10%	**0.9857**	**40.4086**	0.9843	40.0002	**0.9833**	**39.7838**	0.9804	39.1425
sample rate: 20%	**0.9941**	**45.1404**	0.9936	44.3933	**0.9929**	**43.4699**	0.9917	42.7524
sample rate: 30%	**0.9970**	**47.4116**	0.9967	47.3890	**0.9962**	**47.0466**	0.9961	46.1701

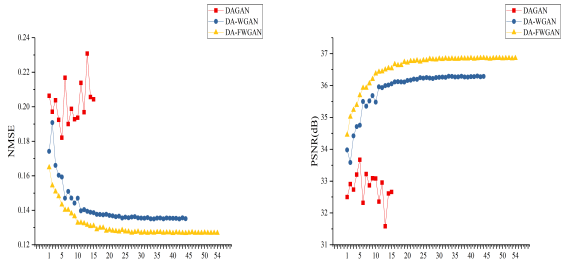

FIGURE 9. The convergences of NMSE (a) and PSNR (b) as a function of epoch for the case of 10% sampling rate with the 1D Gaussian mask.

DA-FWGAN methods are always steady and stable. With increasing epoch, the reconstruction performance gets better and converges gradually to the asymptotic optimal state. The convergence analysis indicates that the fine-tuning method can significantly reduce the training complexity of WGAN with stabilized and fast-converging training.

The proposed DA-FWGAN reconstruction method is a typical end-to-end network structure to generate accurate MRI reconstruction from highly under-sampled k-space data. Compared with other deep-learning based algorithms, the proposed DA-FWGAN method can reconstruct under-sampled MRI data with higher PSNR and SSIM with better preservation of the fine anatomical structures. However, there is still space for further improvement. The DA-FWGAN method in its current form requires relatively long training time and predefined hyperparameters. In the future works, we will test data augmentation to enlarge training samples and include procedures to optimize the hyperparameters.

VI. CONCLUSION

In this paper, an end-to-end MRI reconstruction method, DA-FWGAN, is proposed to perform CS-MRI reconstruction. The method integrates training method of fine-tuning with Wasserstein distance as training criterion. Compared with the other state-of-the-art deep learning reconstruction methods for CS-MRI, such as ADMM-Net, Pixel-GAN, and DAGAN, our experimental results have demonstrated that the proposed DA-FWGAN method can effectively suppress the well-known aliasing artifacts in highly accelerated MRI and reconstruct more accurately with higher PSNR and SSIM. The proposed DA-FWGAN method provides a promising approach to improve MRI time efficiency without sacrificing the image qualities.

REFERENCES

[1] M. Seregni, C. Paganel, P. Summers, M. Bellomi, G. Baroni, and M. Riboldi, "A hybrid image registration and matching framework for real-time motion tracking in MRI-guided radiotherapy," *IEEE Trans. Biomed. Eng.*, vol. 65, no. 1, pp. 131–139, Jan. 2018.

[2] D. G. Nishimura, "Principles of magnetic resonance imaging," Dept. Elect. Eng., Stanford Univ., Stanford, CA, USA, Tech. Rep., 1996.

[3] M. Lakrimi, A. M. Thomas, G. Hutton, M. Kruip, R. Slade, P. Davis, A. J. Johnstone, M. J. Longfield, H. Blakes, S. Calvert, M. Smith, and C. A. Marshall, "The principles and evolution of magnetic resonance imaging," *J. Phys., Conf.*, vol. 286, no. 1, pp. 1–11, 2011.

[4] Y. Han and J. C. Ye, "k-space deep learning for accelerated MRI," 2018, *arXiv:1805.03779*. [Online]. Available: https://arxiv.org/abs/1805.03779

[5] M. Lustig, D. L. Donoho, J. M. Santos, and J. M. Pauly, "Compressed sensing MRI," *IEEE Signal Process. Mag.*, vol. 25, no. 2, pp. 72–82, Mar. 2008.

[6] Z. Lai, X. Qu, Y. Liu, D. Guo, J. Ye, Z. Zhan, and Z. Chen, "Image reconstruction of compressed sensing MRI using graph-based redundant wavelet transform," *Med. Image Anal.*, vol. 27, pp. 93–104, Jan. 2016.

[7] Y. Yang, F. Liu, M. Li, J. Jin, E. Weber, Q. Liu, and S. Crozier, "Pseudo-polar Fourier transform-based compressed sensing MRI," *IEEE Trans. Biomed. Eng.*, vol. 64, no. 4, pp. 816–825, Apr. 2017.

[8] C. Chang, X. Yu, and J. X. Ji, "Compressed sensing MRI reconstruction from 3D multichannel data using GPUs," *Magn. Reson. Med.*, vol. 78, no. 6, pp. 2265–2274, 2017.

[9] Z. Lai, X. Qu, H. Lu, X. Peng, D. Guo, Y. Yang, G. Guo, and Z. Chen, "Sparse MRI reconstruction using multi-contrast image guided graph representation," *Magn. Reson. Imag.*, vol. 43, pp. 95–104, Nov. 2017.

[10] S. Liu, J. Cao, G. Wu, H. Liu, X. Tan, and X. Zhou, "CS-MRI reconstruction via group-based eigenvalue decomposition and estimation," *Neurocomputing*, vol. 283, pp. 166–180, Mar. 2018.

[11] X. Fan, Q. Lian, and B. Shi, "Compressed sensing MRI with phase noise disturbance based on adaptive tight frame and total variation," *IEEE Access*, vol. 5, pp. 19311–19321, 2017.

[12] L. Feng, M. B. Srichai, R. P. Lim, A. Harrison, W. King, G. Adluru, E. V. R. Dibella, D. K. Sodickson, R. Otazo, and D. Kim, "Highly accelerated real-time cardiac cine MRI using $k-{-}t$ SPARSE-SENSE," *Magn. Reson. Med.*, vol. 70, no. 1, pp. 64–74, 2013.

[13] L. Feng, R. Grimm, K. T. Block, H. Chandarana, S. Kim, J. Xu, L. Axel, D. K. Sodickson, and R. Otazo, "Golden-angle radial sparse parallel MRI: Combination of compressed sensing, parallel imaging, and golden-angle radial sampling for fast and flexible dynamic volumetric MRI," *Magn. Reson. Med.*, vol. 72, no. 3, pp. 707–717, 2014.

[14] S. Wang, S. Wang, S. Tan, Y. Gao, Q. Liu, L. Ying, T. Xiao, Y. Liu, X. Liu, H. Zheng, and D. Liang, "Learning joint-sparse codes for calibration-free parallel MR imaging," *IEEE Trans. Med. Imag.*, vol. 37, no. 1, pp. 251–261, Jan. 2018.

[15] Z. Chen, Y. Fu, Y. Xiang, J. Xu, and R. Rong, "A novel low-rank model for MRI using the redundant wavelet tight frame," *Neurocomputing*, vol. 289, pp. 180–187, May 2018.

[16] J. Cao, S. Liu, H. Liu, X. Tan, and X. Zhou, "Sparse representation of classified patches for CS-MRI reconstruction," *Neurocomputing*, vol. 339, pp. 255–269, Apr. 2019.
[17] Y. Huang, J. Paisley, Q. Lin, X. Ding, X. Fu, and X.-P. Zhang, "Bayesian nonparametric dictionary learning for compressed sensing MRI," *IEEE Trans. Image Process.*, vol. 23, no. 12, pp. 5007–5019, Dec. 2014.
[18] Z. Zhan, J.-F. Cai, D. Guo, Y. Liu, Z. Chen, and X. Qu, "Fast multiclass dictionaries learning with geometrical directions in MRI reconstruction," *IEEE Trans. Biomed. Eng.*, vol. 63, no. 9, pp. 1850–1861, Sep. 2016.
[19] Y. Wang, G. Ma, L. An, F. Shi, P. Zhang, D. S. Lalush, X. Wu, Y. Pu, J. Zhou, and D. Shen, "Semisupervised tripled dictionary learning for standard-dose PET image prediction using low-dose PET and multimodal MRI," *IEEE Trans. Biomed. Eng.*, vol. 64, no. 3, pp. 569–579, Mar. 2017.
[20] Y. LeCun, Y. Bengio, and G. Hinton, "Deep learning," *Nature*, vol. 521, pp. 436–444, May 2015.
[21] J. Du, Z. He, L. Wang, A. Gholipour, Z. Zhou, D. Chen, and Y. Jia, "Super-resolution reconstruction of single anisotropic 3D MR images using residual convolutional neural network," *Neurocomputing*, to be published. doi: 10.1016/j.neucom.2018.10.102.
[22] J. Xie, L. Xu, and E. Chen, "Image denoising and inpainting with deep neural networks," in *Proc. Adv. Neural Inf. Process. Syst.*, 2012, pp. 341–349.
[23] B. Zhu, J. Z. Liu, S. F. Cauley, B. R. Rosen, and M. S. Rosen, "Image reconstruction by domain-transform manifold learning," *Nature*, vol. 555, no. 7697, p. 487, 2018.
[24] S. J. Pan and Q. Yang, "A survey on transfer learning," *IEEE Trans. Knowl. Data Eng.*, vol. 22, no. 10, pp. 1345–1359, Oct. 2010.
[25] Z. Zhou, J. Shin, L. Zhang, S. Gurudu, M. Gotway, and J. Liang, "Fine-tuning convolutional neural networks for biomedical image analysis: Actively and incrementally," in *Proc. CVPR*, Jul. 2017, pp. 7340–7351.
[26] T. Chen, X. Song, and C. Wang, "Preserving-texture generative adversarial networks for fast multi-weighted MRI," *IEEE Access*, vol. 6, pp. 71048–71059, 2018.
[27] D. Lee, J. Yoo, S. Tak, and J. Ye, "Deep residual learning for accelerated MRI using magnitude and phase networks," *IEEE Trans. Biomed. Eng.*, vol. 65, no. 9, pp. 1985–1995, Sep. 2018.
[28] S. Wang, Z. Su, L. Ying, X. Peng, S. Zhu, F. Liang, D. Feng, and D. Liang, "Accelerating magnetic resonance imaging via deep learning," in *Proc. IEEE 13th Int. Symp. Biomed. Imag.*, Apr. 2016, pp. 514–517.
[29] J. Schlemper, J. Caballero, J. V. Hajnal, A. N. Price, and D. Rueckert, "A deep cascade of convolutional neural networks for dynamic MR image reconstruction," *IEEE Trans. Med. Imag.*, vol. 37, no. 2, pp. 491–503, Feb. 2017.
[30] Y. Li, N. Xiao, and W. Ouyang, "Improved generative adversarial networks with reconstruction loss," *Neurocomputing*, vol. 323, pp. 363–372, Jan. 2019.
[31] Y. Yang, J. Sun, H. Li, and Z. Xu, "Deep ADMM-net for compressive sensing MRI," in *Proc. 29th Int. Conf. Neural Inf. Process. Syst.*, 2016, pp. 10–18.
[32] J. Yang, Y. Zhang, and W. Yin, "A fast alternating direction method for TVL1-L2 signal reconstruction from partial Fourier data," *IEEE J. Sel. Topics Signal Process.*, vol. 4, no. 2, pp. 288–297, Apr. 2010.
[33] I. Goodfellow, J. Pouget-Abadie, M. Mirza, B. Xu, D. Warde-Farley, S. Ozair, A. Courville, and Y. Bengio, "Generative adversarial nets," in *Proc. NIPS*, 2014, pp. 2672–2680.
[34] P. Isola, J. Y. Zhou, T. Zhou, and A. A. Efros, "Image-to-image translation with conditional adversarial networks," in *Proc. CVPR*, Jul. 2017, pp. 1125–1134.
[35] J. Johnson, A. Alahi, and F.-F. Li, "Perceptual losses for real-time style transfer and super-resolution," in *Proc. Eur. Conf. Comput. Vis.*, 2016, pp. 694–711.
[36] G. Yang, S. Yu, H. Dong, G. Slabaugh, P. L. Dragotti, X. Ye, F. Liu, S. Arridge, J. Keegan, Y. Guo, and D. Firmin, "DAGAN: Deep de-aliasing generative adversarial networks for fast compressed sensing MRI reconstruction," *IEEE Trans. Med. Imag.*, vol. 37, no. 6, pp. 1310–1321, Jun. 2018.
[37] M. Arjovsky, S. Chintala, and L. Bottou, "Wasserstein GAN," 2017, *arXiv:1701.07875*. [Online]. Available: https://arxiv.org/abs/1701.07875
[38] Q. Yang, P. Yan, Y. Zhang, H. Yu, Y. Shi, X. Mou, M. K. Kalra, Y. Zhang, L. Sun, and G. Wang, "Low-dose CT image denoising using a generative adversarial network with Wasserstein distance and perceptual loss," *IEEE Trans. Med. Imag.*, vol. 37, no. 6, pp. 1348–1357, Jun. 2018.
[39] V. Antun, F. Renna, C. Poon, B. Adcock, and A. C. Hansen, "On instabilities of deep learning in image reconstruction—Does AI come at a cost?" 2019, *arXiv:1902.05300*. [Online]. Available: https://arxiv.org/abs/1902.05300
[40] O. Ronneberger, P. Fischer, and T. Brox, "U-net: Convolutional networks for biomedical image segmentation," in *Proc. Med. Image Comput. Comput.-Assist. Intervent.*, 2015, pp. 234–241.
[41] Y. Han and J. C. Ye, "Framing U-net via deep convolutional framelets: Application to sparse-view CT," *IEEE Trans. Med. Imag.*, vol. 37, no. 6, pp. 1418–1429, Jun. 2018.
[42] H. Dong, G. Yang, F. Liu, Y. Mo, and Y. Guo, "Automatic brain tumor detection and segmentation using U-net based fully convolutional networks," in *Proc. Annu. Conf. Med. Image Understand. Anal. Commun. Comput. Inf. Sci.*, 2017, pp. 506–517.
[43] L. Rüschendorf, "The Wasserstein distance and approximation theorems," *Probab. Theory Rel. Fields*, vol. 70, no. 1, pp. 117–129, 1985.
[44] J. Adler, A. Ringh, O. Oktem, and J. Karlsson, "Learning to solve inverse problems using Wasserstein loss," 2017, *arXiv:1710.10898*. [Online]. Available: https://arxiv.org/abs/1710.10898
[45] E. M. Eksioglu, "Decoupled algorithm for MRI reconstruction using nonlocal block matching model: BM3D-MRI," *J. Math. Imag. Vis.*, vol. 56, no. 3, pp. 430–440, Nov. 2016.
[46] I. Gulrajani, F. Ahmed, M. Arjovsky, V. Dumoulin, and A. C. Courville, "Improved training of Wasserstein GANs," in *Proc. NIPS*, 2017, pp. 5767–5777.
[47] M. Arjovsky and L. Bottou, "Towards principled methods for training generative adversarial networks," in *Proc. ICLR*, 2017, pp. 1–17.
[48] O. Russakovsky, J. Deng, H. Su, J. Krause, S. Satheesh, S. Ma, Z. Huang, A. Karpathy, A. Khosla, M. Bernstein, A. C. Berg, and F. Li, "ImageNet large scale visual recognition challenge," *Int. J. Comput. Vis.*, vol. 115, no. 3, pp. 211–252, Dec. 2015.

MINGFENG JIANG received the B.S. and M.S. degrees in biomedical engineering from Chongqing University, China, in 2000 and 2003, respectively, and the Ph.D. degree in biomedical engineering from Zhejiang University, China, in 2008. From 2011 to 2012, he was a Visiting Scientist with the Department of Electrical Engineering, University of Queensland, Australia. He is currently a Professor with the School of Information Science and Technology, Zhejiang Sci-Tech University, China. His research interests include biomedical signal processing, MR image reconstruction, and inverse ECG problem.

ZIHAN YUAN received the B.S. degree in computer science and technology from Zhengzhou University, Zhengzhou, Henan, in 2017. He is currently pursuing the master's degree with Zhejiang Sci-Tech University, Hangzhou, Zhejiang. His research interests include deep learning and MR image reconstruction.

XU YANG received the B.S. degree in optical information science and technology and the Ph.D. degree in physics from the Harbin Institute of Technology, Harbin, China. Since 2018, he has been with the School of Information Science and Technology, Zhejiang Sci-Tech University, where he was a Lecturer. His research interests include computation imaging, deep learning, and compressed sensing.

JUCHENG ZHANG received the B.S. degree in communication engineering from Yantai University, China, in 2010, and the M.S. degree in signal and information processing from China Jiliang University, China, in 2013. He is currently an Engineer of the Second Affiliated Hospital, School of Medicine, Zhejiang University, China. His research interests include biomedical signal processing and MR image reconstruction.

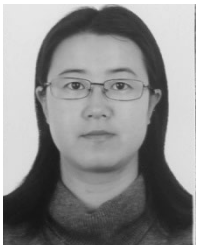

YINGLAN GONG received the B.S. and M.S. degrees in biomedical engineering from Tianjing Medical University, China, in 2000 and 2005, respectively, and the Ph.D. degree in biomedical engineering from Zhejiang University, China, in 2012. She is currently a Research Fellow of the Institute of Biomedical Engineering, Zhejiang University. Her research interests include heart modeling and simulation, and biomedical signal processing.

LING XIA received the B.S. degree in electrical automation control and the Ph.D. degree in biomedical engineering from Zhejiang University, Hangzhou, China, in 1987 and 1996, respectively. He is currently a Professor and the Vice Director of the Institute of Biomedical Engineering, Zhejiang University. His current research interests include the multiscale heart modeling and simulation, ECG inverse problem, MRI key technology, and biological effect of electromagnetic field.

TIEQIANG LI received the B.S. degree from the Department of Chemical Engineering, Tianjin University of Science and Technology, Tianjin, China, in 1983, and the Ph.D. degree from the Faculty of Chemistry and Chemical Technology, Royal Institute of Technology, Stockholm, Sweden, in 1997. He is currently a R&D Responsible for the MRI Physics Unit, Department of Medical Radiation Physics and Nuclear Medicine, Karolinska University Hospital, Huddinge, Stockholm. His current research interests include developing rapid data acquisition methods, and novel post-processing techniques for MRI and exploring new imaging contrast mechanisms for neurological applications.